ORIGINAL ARTICLE

Journal Section

Nonsubsampled contourlet transform based tone mapping operator to optimize the dynamic range of diatom shells

Harbinder Singh PhD[1*] | Gabriel Cristobal PhD[2] | Saul Blanco PhD[3] | Gloria Bueno PhD[4] | Carlos Sanchez PhD[2,4]

[1]Chandigarh Engineering College, Department of Electronics and Communication Engineering, Landran, Mohali, India.

[2]Instituto de Optica(CSIC), Serrano 121, 28006 Madrid, Spain

[3]University of Leon - Universidad de Leon, Department of Biodiversity and Environmental Management, Spain

[4]VISILAB, Univ. Castilla la Mancha, Cuidad Real, Spain

Correspondence
Corresponding author at: Chandigarh Engineering College, Department of ECE, Landran, Mohali, India.
Email: harbinder.ece@gmail.com

Funding information

The diatoms have intricate silica-based cell walls with multi-scale patterns. High Dynamic Range (HDR) imaging is widely used to examine the 3D structure of diatoms for recovering the wide range of contrast and brightness. In order to construct a HDR image of a diatom, multiple images of the specimen are taken at different exposure settings with bright or dark field microscopy. In the proposed method, multi-scale decomposition (MSD) based on Nonsubsampled Contourlet Transform (NSCT) is adopted to separate the structured and detailed information of the HDR image. And then, by processing all layers independently, the tone mapped image is reconstructed to retain details present in the dark and light regions. Quantitative and qualitative analysis is performed in order to assess the performance of the proposed and 7 existing Tone Mapping Operators (TMOs). In analysis, the study indicates that the proposed method enhances the diatom frustules to extract more details.

Research Highlights

1. Tone mapping approach is proposed for HDR microscopy images of diatom species.
2. The approach is based on NSCT based multi-scale decomposition.
3. The lowpass and directional high frequency subbands of HDR images are processed separately for preserving details present in the dark and bright regions.
4. The fine structures and contours of diatom frustules are enhanced that can be used for identification and classification of different species.

KEYWORDS
Diatom, HDR, Microscopy, Multi-exposure, Tone Mapping

1 | INTRODUCTION

As the demand for HDR imaging to capture and store more data increases, multi-exposure photography is compelled to extract details from a scene with wide range of luminance and contrast [1]. HDR imaging has been adapted in different application scenarios such as computer graphics, generation of realistic images, military applications and medical imagery. The technique of taking multiple shots of the same specimen at different exposure values is called exposure bracketing [2]. As a consequence, several HDR construction algorithms have been developed for merging multi-exposure images of real world scene to avoiding under-exposed and over-exposed regions [3, 4, 5]. For the construction of HDR images, several freeware stacking software with integrated rendering features have been also designed [6, 7, 8, 9]. Although these HDR construction techniques seem to recover dynamic range from real world scenes, they still suffer from ghost-like artifacts due to the object movements in a scene and imaging device during the capture of images at various exposure levels. To overcome this problem, inverse tone mapping approach based on Convolutional Neural Networks (CNNs) is developed [10]. They proposed a method in which HDR image is constructed from a single image. A tone mapping operator based Low Dynamic Images (LDR) is predicted for HDR construction. However, tone mapping operators are expected to be developed for HDR imaging. The important characteristics of different HDR stacking software tested on microscopic data sets are discussed in [11]. Diatoms are one of the most plentiful microalgae with nano- and micro-patterns housed in all aquatic regions across the world. The microscopic investigation of complex silica-based cell walls of diatom species have motivated the researchers to develop imaging techniques for cell structure characterization and identification of different species [12], [13]. When a specimen such as diatom with 3D transparent structures are photographed with the help of brightfield or darkfield microscopy, only a limited range of visible contrast and brightness are exposed properly [11]. In this case, poorly illuminated areas may appear under-exposed than brightly illuminated areas that may appear over-exposed. Therefore, in most cases, entire range of the luminance can not be covered in a single shot. Because of this reason, to cope with the entire range of luminance variation, the specimen needs to be captured at different exposure settings for detailed analysis of fine structures [14]. In digital photomicrography, [11] propose to use up to ISO 400 according to the brightness level of

the specimen when bridge digital cameras are available. And for reducing the noise level in the multi-exposure images, he has recommenced to prefer up to ISO 1600 or ISO 3200 when a digital mirror reflex cameras are used. Therefore, special HDR construction and tone mapping methods are also needed to capture more details from multi-exposure images taken with the help of bright or dark-field microscopy.

Similar to the image recording devices, the same restriction exists in conventional display devices such as traditional cathode ray tube (CRT) or liquid crystal diode (LCD) monitors, projectors and printers that can not visualize the HDR content. The maximum display luminace of a properly designed CRT is close to 100 cd m^{-2} and for an LCD it can vary from 250 to 500 cd m^{-2}. Therefore, when displaying HDR images on such display devices, the dynamic range needs to be compressed using tone mapping operators [15]. Researchers have categorized the tone mapping operators (TMOs) into two categories that includes Local TMOs and Global TMOs. In Local TMOs, the local content adaptive mapping function is applied at each pixel location that helps to preserve minute local details, but introduce halos near strong edges and also make the process computationally expensive. [16] used spatially varying compression functions that is derived from the average of neighbouring pixels. It utilizes the concept of Global TMOs but still suffers from artifacts near strong edges. A different approach was used by [17] that is inspired from photographic principles. It utilizes spatially varying Gaussian kernels to identifying the areas without edge details and does not introduce halos. In another work, a two-scale decomposition based on bilateral filter [1] was used to preserve details in the resultant tone mapped image. The tone mapping function was applied on base layer without altering the detail layer. The final tone mapped image was reconstructed from the modified base layer, detail layer and chrominance details. But this method also suffered from the halos problem near strong edges. To improve the performance of two-scale decomposition based tone mapping approach proposed by [1], the bilateral filter filter was replaced by a trilateral filter [18]. To reducing the impact of strong noise and rejecting the outlier, they utilizes edge-limited smoothing capabilities of shock-forming partial differential equations. A more recent method has provided insights into how weighted least squares (WLS) [19] can be utilized to avoiding artefacts in two-scale decomposition based tone mapping processes [20].

[21] presented a method for dynamic range compression that was based on gradient field manipulation by compressing the magnitude of strong gradients. This method was able to preserve details and avoiding the gradient reversal artifacts. An improvement was proposed by [22] in which gradient manipulation was done block by block using real-time Discrete Sine Transform. It was implemented on hardware for real-time video applications. On the other hand, in Global TMOs the same mapping function was applied at each pixel location in the HDR image that makes it computationally simple and efficient. The Global TMOs also introduces fewer artifacts than the Local TMOs . [4] has proposed an histogram adjustment based tone mapping function that utilizes the human color sensitivity, contrast sensitivity, and spatial acuity. It was proposed by [23] that histogram of luminance can be employed to guide the tone mapping operation. [24] proposed an adaptive logarithmic bias power mapping function to compressing luminance values. A TMO operator based on limit curve guided by perceptual quantization was proposed by [25] that enhances the contrast in the output image. To compress the dynamic range of HDR image [26] has utilized sigmoidal curve that is based on the response curve of retina. A Human Visual System (HVS) model based viability prediction was proposed by [27] to preserve important details and contrast in the resultant tone mapped image.

As the nano- and micro-patterns of diatom species are important for cell structure characterization and identification of different diatom species, it would seem obvious that tone mapping operator should utilize multi-scale decomposition. To do so, structured layer and detailed layers are constructed using NSCT [28] that separates the structure and fine details of the HDR image. The lowpass subband contain the structured information and bandpass directional subbands describe the detailed information. Unlike the most existing tone mapping operators, we do not apply tone mapping process on the input HDR image. Instead, we adopt local gain maps to modify the bandpass

TABLE 1 Properties of 10 microscopy multi-exposure image data sets acquired using darkfield and brightfield microscopy.

Image	Exposure time (seconds)	Dimensions	Imaging
Pinnularia sp.	1/200, 1/100, 1/50, 1/25	3456×5184	Brightfield
Stauroneis gracilis	1/20, 1/5, 1/2, 1.29	5184×3456	Darkfield
Lyrella sp.	1/25 1/8, 1/3, 1	5184×3456	Darkfield
Triceratium favus	1/160, 1/100, 1/60, 1/30	2552×1728	Brightfield
Stauroneis gracilis and Lyrella sp.	1/400, 1/200, 1/100, 1/50, 1/25	5184×3456	Brightfield
Pleurosira sp.	1/250, 1/125, 1/60, 1/30, 1/15	2552×1728	Brightfield
Frustulia saxonica	1/250, 1/125, 1/60, 1/30, 1/15	1920×1080	Brightfield
Lyrella sp. in-focus	1/250, 1/125, 1/60, 1/30, 1/15	2552×1728	Brightfield
Gyrosigma cf. balticum	1/250, 1/125, 1/60, 1/30, 1/15	2552×1728	Brightfield
Surirella gemma	1/250, 1/125, 1/60, 1/30, 1/15	2552×1728	Brightfield

directional subbands for tonal range manipulation. The tonal range of lowpass subband is altered separately. To get a final tone-mapped image using inverse NSCT, the modified bandpass directional subbands are recombined to the manipulated lowpass subband. Experimental results show that the proposed approach leads to consistent enhancement of the details in the tone mapped images.

2 | DYNAMIC RANGE OPTIMIZATION BY TONE MAPPING OPERATOR

2.1 | Data set collection

All multi-exposure image stacks were photographed with a Canon EOS 1300D, 18MP Digital SLR Camera mounted on a Brunel SP500, Objective 60X, NA 0.85. Ten multi-exposure data sets of diatom species are collected under the supervision of two expert diatomists. Detailed properties of all acquired image stacks are given in the Table 1. Due to space constraints, multiexposure image series is demonstrated for two data sets (see Fig. 1). The remaining eight data sets are provided as supplementary material separately.

In the first data sets of "*Pinnularia sp.*" shown in Figs. 1 (a-d), a series of four multi-exposure images is acquired using brightfield illumination. We can observe low contrast structures in the data sets of "*Pinnularia sp.*", and the fine details within a transparent structures are hardly recognizable. The number of exposures per data set necessary for perfect HDR construction is dependent on the range of intensity variations present in the specimen under the observation. All necessary details within the specimen should be exposed properly at least in the one of the exposure. The captured multi-exposure stacks were size of 3456×5184 with bit depth, field of view, and fixed focal length of 8, 25.8 deg., and $50\,mm$, respectively. The exposure times of multi-exposure images acquired were $1/200\,s$, $1/100\,s$, $1/50\,s$ and $1/25\,s$ with an ISO setting of 100. In a similar way, we have acquired a second data set of "*Stauroneis gracilis*" using darkfield illumination. The exposure times of multi-exposure images acquired were $1/20\,s$, $1/5\,s$, $1/2\,s$ and $1.29\,s$. We can notice from multi-exposure images shown in Figs. 1 (e-c) fine structures in the silica frustule are better recognizable at different exposure settings. Furthermore, due to different illumination effects, specimen produces ultra-high contrast within a transparent structures. Therefore, these multi-exposure images of specimen

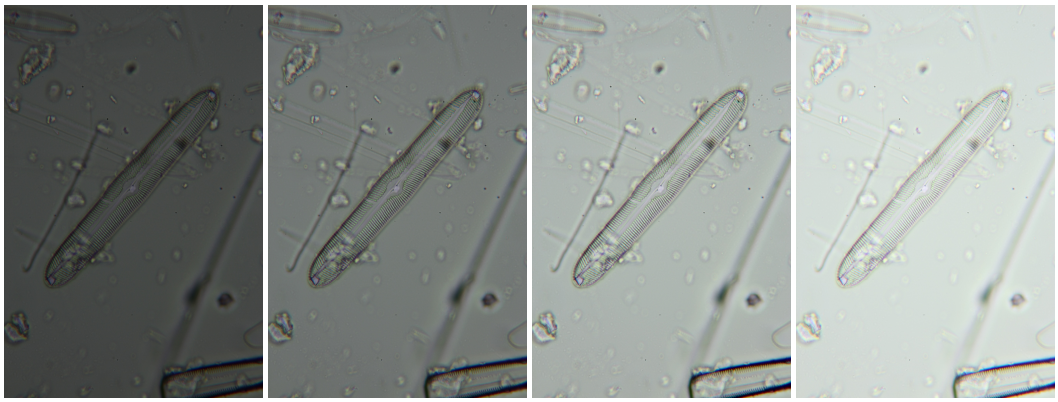

(a) 1/200 *s* (b) 1/100 *s* (c) 1/50 *s* (d) 1/25 *s*

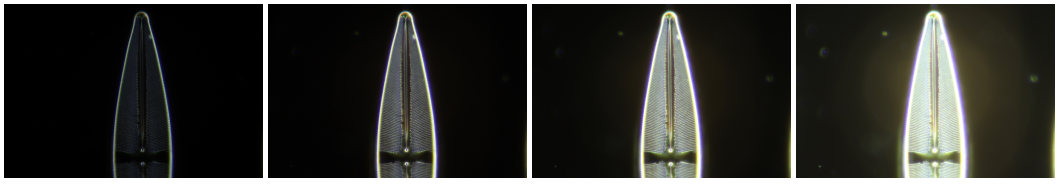

(e) 1/20 *s* (f) 1/5 *s* (g) 1/2 *s* (h) 1.29 *s*

FIGURE 1 Multi-exposure image Series: (a-d) Multi-exposure images of "*Pinnularia sp.*", and (e-h) Multi-exposure images of "*Stauroneis gracilis*" diatom species.

can be used to construct HDR image, so that fine structures are enhanced furthermore.

2.2 | HDR construction

Let there are N multi-exposure images of a specimen, with exposure values t_i, $i = 1, ..., N$. The pixel value of i^{th} image at j^{th} spatial location is denoted by Z_{ij}. The goal of HDR construction is to recover irradiance values E_i based on camera response function (CRF) $f(\cdot)$ [17]. The output values using known CRF function is given by

$$Z_{ij} = f(E_i\, t_i) \tag{1}$$

To estimate the E_i values having high dynamic range, we can rewrite equation 1 as:

$$f^{-1}(Z_{ij}) = E_i\, t_i \tag{2}$$

From equation 2, E_i is computed in the logarithmic domain that is given by

$$In\, E_i = In\, f^{-1}(Z_{ij}) - In\, t_i \tag{3}$$

[3] addressed the least squared solution to compute the function ($g = Inf^{-1}$) and the irradiance values E_i. In this paper, the method of [3] is used to construct HDR images of the specimen photographed in bright-field and darkfield at different exposure values.

2.3 | Problem Formulation

Given an HDR image E, a tone mapping operator compresses the luminance values to produce low dynamic range (LDR). Owing to the multi-band, multi-direction, and shift-invariant property of NSCT, it is employed on input HDR image of the diatom species for multi-scale decomposition. To preserve details associated with a complex silica-based cell walls of diatom species, we compress the dynamic range of each band using gain-control function. The gain-control function for ideally bandpass directional subbands are computed from the lowpass subband. To get better results we modify the lowpass subband separately, and recombined with the modified bandpass directional subbands during the reconstruction process. The proposed model manipulate the tonal range of input HDR image, while still better preserves the abundant delicate cell structure of diatom species. Let $b^H_{j0}(x, y)$ and $b^H_{j,l}(x, y)$ are the low-pass subband and bandpass directional subbands computed across the luminance channel L of input HDR image, respectively. Where $b^H_{j,l}(x, y)$ is the bandpass directional subband obtained at the j_{th} scale in the l_{th} direction. The luminance channel L is obtained from the red R, green G, and blue B color channels that is given by

$$L = 0.2126 \times R + 0.7152 \times B + 0.0722 \times G \tag{4}$$

In the forthcoming paragraphs, we will briefly explain the multi-scale decomposition of our TMO.

2.4 | Nonsubsampled Contourlet Transform

NSCT is a shift-invariant transform that is based on nonsubsampled pyramid structure and nonsubsampled filter banks. In addition to shift-invariance property, due to better frequency selectivity it provides more desirable multi-scale image decomposition [28]. The building block of NSCT is shown in Fig. 2 (a). For three-level decomposition, the frequency partitioning on the 2-D frequency plane is illustrated in Fig.2 (b).

NSCT's multiscale property is accomplished by the use of two-channel non-sampled 2-D filter banks (NSFBs) that are called nonsubsampled pyramid filter (NSP) bank (NSPFB) [28]. The next-level filters are obtained by upsampling the previous-level filters, from which the multiscale property is obtained without the need for additional filter architecture. At each level, one low-frequency subband and one high-frequency subband is produced by NSP. Therefore, NSP results in $k + 1$ sub-bands, consisting of one low-and k high-frequency bands of the same size as the input where k represents the amount of degrees of decomposition. For further decomposition, nonsubsampled directional filter bank (NSDFB) decomposes the high-frequency subband into several directional subbands. As for a particular subband, let the number of directions for decomposition be l; then obtain 2^l directional subbands, whose sizes are identical to the input image. If we denote the analysis low-pass filter and high-pass filter by $H_0(z)$ and $H_1(z) = 1 - H_0(z)$ respectively, then the corresponding synthesis filters can be $G_0(z)$ and $G_1(z)$. The perfect reconstruction can be obtained that imposes the *Bezout's identity* [28] as follows

$$H_0(z)G_0(z) + H_1(z)G_1(z) = 1 \tag{5}$$

The key benefits of NSCT over other multiscale decomposition is that at each scale the contourlet transform

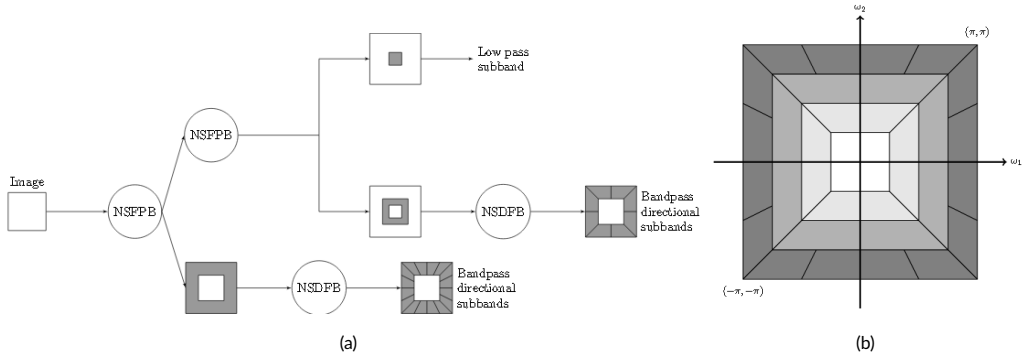

FIGURE 2 Nonsubsampled contourlet transform (NSCT). (a) NSFB structure, which implements the NSCT.(b) Depiction of frequency partitioning on the 2-D frequency plane.

allows for specific and customizable number of directions. In addition, it has important features such as smooth contour edge detection, shift-invariant and fast implementation [28]. In the proposed algorithm, the HDR image is decomposed into multiscale decomposition using $H_0(z)$ and corresponding $H_1(z)$ into lowpass and highpass subbands, respectively. After 4-level decomposition, one low pass band and a sequence of 8 directional high frequency subbands are obtained. To preserve information associated with the cell walls of diatom species, we have devised a new detail-preserving contrast reduction hierarchy. Applying the same contrast reduction function for coarser and detail layers one may compress the contrasts sufficiently, but also remove important details will be removed. In the proposed hierarchy, different contrast reduction functions are used for lowpass band and high frequency subbands. The architecture of the proposed NSCT based tone mapping algorithm is shown in Fig. 3. In first step the input HDR image is decomposed into subbands that describe the structured and detailed features of source image. In second step, different gain map functions are employed to the subbands for tone mapping. In the final step, inverse NSCT transform is applied on modified subbands to reconstruct tone mapped image with improved visual perception. Furthermore, the color channel regulation can be carried out to accentuate the fine structures and contours of diatom frustules. In particular, color modification is useful when sophisticated polarizing filters such as “vario-color” or “pol-color” filters are utilized to photograph transparent colored specimen [29]. The proposed gain map computation, and tone mapping process is discussed in the forthcoming section.

2.5 | A Novel NSCT Domain Tone Mapping

As described in the previous section, it is advantageous to use different contrast reduction functions for lowpass band and high frequency subbands. Diatom images contain an abundance of details with different orientations at multiple scales. In these subbands, High frequency subbands yield detailed information such as edges, lines and corners. Therefore we must use a gain map to accurately manipulate the tonal range of all subbands. Based on the Human Visual System (HVS) model, we focus on the facts of photoreceptor adaptive properties to propose our NSCT based TMO (NT-TM).

[30] reviews the cat striate cell response mechanism. Based on the model described in such paper, in daily life the HVS faces a significant challenge with dynamic range. The striate cortex cells have mechanism for energy normalisation to meet this challenge. Adaptive gain control mechanism is adopted in this energy normalisation phase to

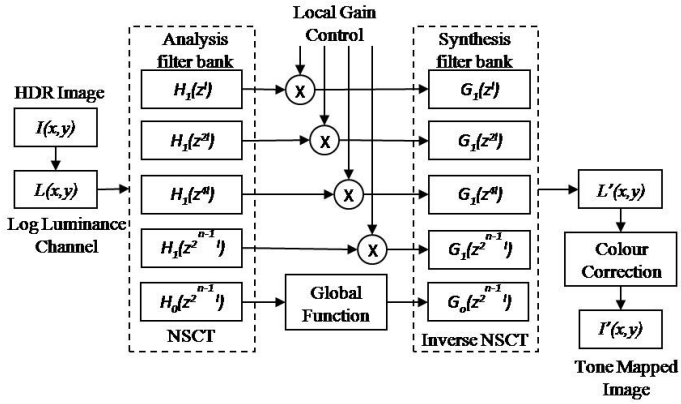

FIGURE 3 Architecture of proposed NSCT based tone mapping (NT-TM) approach.

improve the response of low energy cells, while attenuating the response of high energy cells. Based on the energy level of cells tuned to various orientations and spatial frequencies, the control process differs and is analogous to the processing of the image subbands using adaptive gain maps. A method for dynamic range compression was patented by [31] in which gain control maps are used to modify the contrast of detail layers, and different tone mapping function are used for coarse layer. The NT-TM approach suggested in this paper adopts a similar type of gain control process but with additional advantage of better frequency selectivity and consistency using NSCT based directional subbands decomposition. It will help to preserve the higher dimensional singularities present in the delicate cell structure of diatom species, and effectively reducing artifacts due to the pseudo-Gibbs phenomenon in the tone mapped (TM) image.

In order to compute gain maps, we begin by computing the activity function A_i from one low pass band and a sequence of eight directional high frequency subbands of HDR image using Gaussian kernel $g(bi, \sigma)$:

$$A_i(x, y) = g(\sigma) * |b_i(x, y)| \tag{6}$$

where b_i denotes the subbands (assuming $i = 1, 2.....9$) which were obtained using NSCT and σ is the scale parameter that defines the width of the Gaussian. The parameter σ is set empirically and varying in accordance with the scaling parameter used in the NSCT decomposition. The smaller value of σ is chosen at the finest scale for retaining information, and the value has increased by a factor of 2 at each scale. Therefore, we compute different activity functions at each scale.

To improve stability in the gain maps, the aggregated function is estimated from all activity maps. It will help to avoid artifacts in the TM image by exploiting the correlation between different subbands. Similar to the cell response model by [30] in which feedback signal is computed from all orientations and nearby spatial frequencies, averaged over space and time, we compute the aggregated maps as follows

$$A'(x, y) = \sum_{i=1,2..9} A_i(x, y) \tag{7}$$

Let $G(x, y)$ denotes the gain map function in which the pixels of larger luminance value are attenuated and the pixels of smaller luminance value are slightly enhanced. Such gain maps function at location (x, y) can be obtained by

$$G(x, y) = \left(\frac{A'(x, y) + \epsilon}{\beta} \right)^{(\gamma - 1)} \tag{8}$$

where ϵ is a regularization parameter that is determining the noise level in the gain map function, and γ (assuming $0 < \gamma < 1$) is an another constant called encoding gamma with compressive power-law nonlinearity. In order to control the stability in the gain map function, we utilize a self-adjusting parameter α_i at each scale. Therefore, the gain map function computed in 8 is used to modify all subbands as follows

$$b_i'(x, y) = \alpha_i G(x, y)) \times b_i(x, y) \tag{9}$$

where the value of α_i is self-adjusting and increases as the spatial frequency increases in the subbands. We compute the α_i similar to the approach suggested by [32].

2.5.1 | Detail Manipulation

The NT-TM operator can be used for boosting details of diatom shells in a very significant manner that utilize a modified sigmoidal function $sig(G, a_1, a_2)$, which is given by

$$sig(G) = \frac{1}{1 + e^{-(G - a_1)/a_2}} \tag{10}$$

where G is a gain maps function computed from 8 that is inputted to the sigmoidal function, a_1 defines the center of the function, and a_2 defines the width of the function. a_1 and a_2 are used as boosting factors to control the detail enhancement. Applying the simple gamma function with tone mapping factor of 0.25 to the structured layer, and enhancing the gain maps function using 10 for the detailed layers leads to further enhancement of details in the resultant tone mapped image. We have found that the parameter selection of $a_1 = 0.1$ and $a_2 = 0.05$ is suitable for detail enhancement in the tone mapped images. In this way, gain map functions are used to modify the contrast of directional high frequency subbands, and different tone mapping curve is used for lowpass subband, which offers more flexibility at tone manipulation.

Finally, the tone mapped image is obtained from the modified lowpass and directional high frequency subbands using the corresponding synthesis filters in NSCT domain [28].

3 | SIMULATION RESULTS AND PERFORMANCE ANALYSIS

3.1 | Visual Evaluation

For visual quality assessment, we have tested our algorithm on two HDR images of diatom species having different characteristics, which include different silica nano-scale and micro-scale patterns. Compared with first image data set of "*Pinnularia sp.*", the second image data set of "*Stauroneis gracilis*" has wide range of intensity variations with fine microstructures. The multiexposure images are shown in Fig. 1.

Reconstruction of such intricate patterns using HDR and tone mapping can be of great interest for the character-

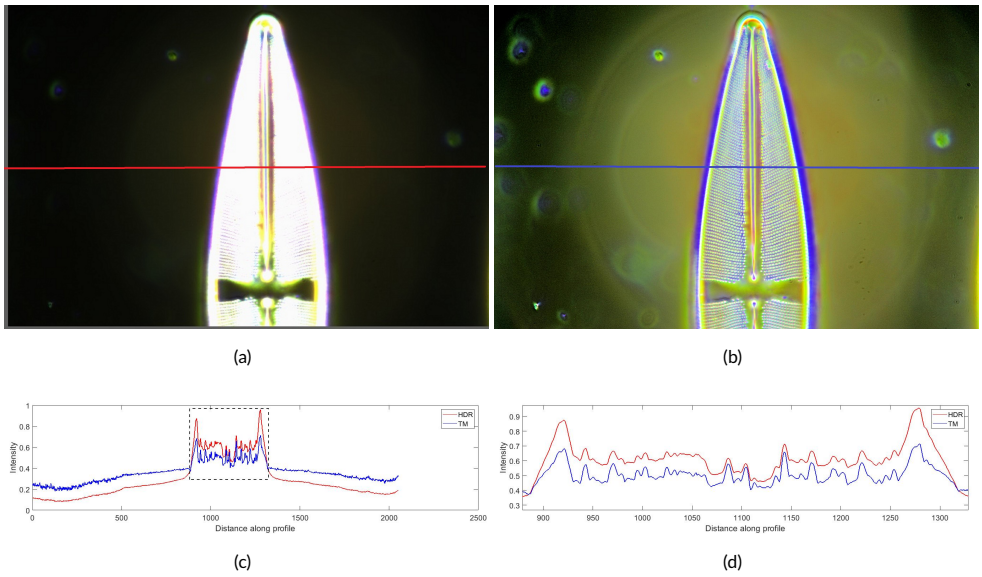

FIGURE 4 Intensity profiles of HDR image and NT-TM image. (a) HDR image with dynamic range of ~ 11 exposure value (EV), (b) NT-TM image with dynamic range of 8 exposure value (EV), (c) Intensity profiles, (d) A closeup of Intensity profiles of region-in-interest in (c).

ization and identification of structural organization. More recent work [33] has reported the role of real time imaging for the identification of species based on symmetry of distinct silica structures and frustule morphology. Indeed, the perfect reconstruction of structural features in a TM image from HDR image has a great importance. The intensity profile of luminance channel of HDR image and NT-TM image without detail manipulation along a scan line is shown in Fig. 4 (c). For better comparison, the closeup of intensity profiles is shown in Fig. 4 (d). We can notice that the locations of peaks and valleys in red plot (HDR image) and blue plot (NT-TM image) are perfectly aligned. It indicates how the intensity values refer to the HDR picture in the tone mapped image. Furthermore, because of better frequency selectivity and consistency using NSCT based subband decomposition, the proposed solution is suitable for detail enhancement in the tone mapped image that is discussed in Section 2.5.1.

The proposed NT-TM is compared with seven existing state-of-the-art methods including commercial HDR software: weighted least squares based TMO (WL-TM) [19], gradient domain TMO (GR-TM) [21], guided filter based TMO (GU-TM) [34], quadrature mirror filters based TMO (QM-TM) [32], bilateral filter based TMO (BL-TM) [1], Hybrid L1-L0 based TMO (HL-TM) [35] and Photomatix Essentials (PM) [6]. All six TMOs are based on multi-layer decomposition, except software technique PM. The results were generated for all TMOs using MATLAB codes, which were made available online by the authors.

TM HDR images of "*Pinnularia sp.*" and "*Stauroneis gracilis*" are selected for visual quality assessment. Fig. 5 and 6 show experimental results of TM images generated by the eight methods including proposed NT-TM. As shown in Figs. 5 (c,d,e) and 6 (c,d,e), the results of WL-TM, GU-TM and BL-TM have not preserved local contrast in the fine structures within the specimen. The results of HL-TM, GR-TM and PM shown in Figs. 5 (a,b,f) and 6 (a,b,f) have better overall contrast but the results of PM do not preserve structural details in the regions with very large intensity variations. As a comparison, the results of QM-TM (see Figs. 5 (g) and 6 (g)) led to better contrast and show more fine details

but could not eliminate blooming associated within transparent regions illuminated by intense light. Moreover, we can notice from Fig. 5 (g) that some structures are not present in the under-exposed regions. From Figs. 5 (h) and 6 (h), it can be noticed that the proposed TMO preserves better structural information, and color details are improved significantly than the other TMOs. For better visual evaluation, a closeup of local regions that are placed at the bottom of different tone mapped images as shown in Figs. 5 and 6. For a better comparison, a closeup of luminance channel of "*Pinnularia sp.*" is demonstreted in Fig. 5. A close inspection reveals that NT-TM can preserve details with better local contrast. In particular, the balance between brightness and contrast is maintained in the diatom frustules with better clarity, while avoiding objectionable artifacts. Due to space limit, visual inspection is demonstrated for two data sets. Furthermore, readers are encouraged to download the supplementary material for qualitative evaluation, which is available on the web link `https://doi.org/10.6084/m9.figshare.12768335`.

3.2 | Objective Analysis

In addition to visual evaluation, three objective performance metrics are used for quantitative analysis. We evaluate the quality of TM HDR images of diatom species using tone-mapped image quality index (TMQI) which was proposed by [36]. It is the revised version of metric based on Multi Scale Structural Similarity Index (MS-SSIM). We first review the TMQI metric that composes two factors i.e. Structural Fidelity (SF) and Statistical Naturalness (SN). A high quality TM HDR image maintains balance between these two factors. For HDR image (H) and TM image (T), the TMQI metric is defined as

$$TMQI(H,T) = a[SF(H,T)]^{\tau_1} + (1-a)[SN(T)]^{\tau_2} \tag{11}$$

where τ_1 and τ_2 define the sensitivity of SF and SN, respectively, and the values of these two parameters are set empirically to $\tau_1 = 0.3046$ and $\tau_2 = 0.7088$. The another constant i.e. a is also set empirically to $a = 0.8012$.

Due to the presence of intricate silica-based cell walls with multi-scale patterns, SF is an important metric to evaluate the quality of a TM HDR image. SF analyse the local structure variation across space. For a local patch r, it is defined as

$$SF(H(r),T(r)) = \frac{2\sigma^{'}(H(r)).\sigma^{'}(T(r)) + C_1}{\sigma^{'2}(H(r)) + \sigma^{'2}(T(r)) + C_2} \times \frac{\sigma^{''}(H(r),T(r)) + C_2}{\sigma^{''}(H(r)).\sigma^{''}(T(r)) + C_2} \tag{12}$$

where $\sigma^{'}$ represents the standard deviation computed after nonlinear mapping; $\sigma^{''}(H(r),T(r))$ and $\sigma^{''}(H(r)), \sigma^{''}(T(r))$ are the cross correlation and local standard deviation computed between the two corresponding local regions in HDR and tone mapped LDR images, respectively; and C_1, C_2 are positive regularization constants.

In comparison to the first part of $TMQI$ (see Eq. 11), SN is a non-reference metric and has less importance in microscopic images. But being a part of $TMQI$, we have considered it as performance measure. It is based on the assumption that the naturalness of gray-scale image can be modelled by the distribution of likelihood of brightness and contrast. A Beta (B) and Gaussian (N) distribution are used to model the standard deviations and means, respectively. For these two mutually independent variables, the SN is defined as

$$SN(T) = \frac{1}{K(T)} \times Pdf_N(T) \times Pdf_B(T) \tag{13}$$

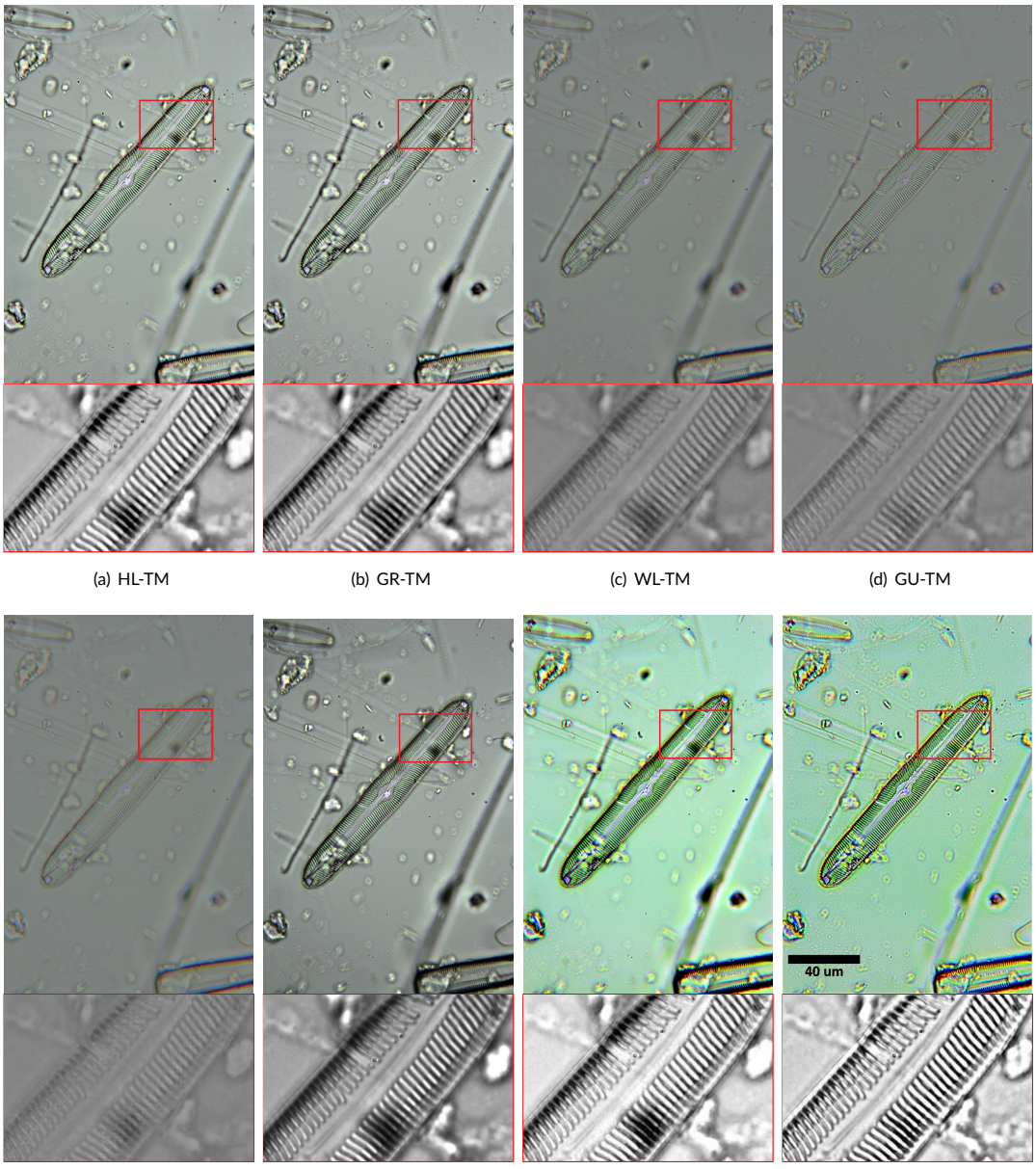

(a) HL-TM (b) GR-TM (c) WL-TM (d) GU-TM

(e) BL-TM (f) PM (g) QM-TM (h) NT-TM

FIGURE 5 Visual comparison of six state-of-the-art TMO, and one commercial HDR and tone mapping tool for "*Pinnularia sp.*" diatom species. To compare the lamellate structures of frustules, the closeup of luminance channel are placed at the bottom of different tone mapped images so that contours and fine structures can be visualized with better precision.

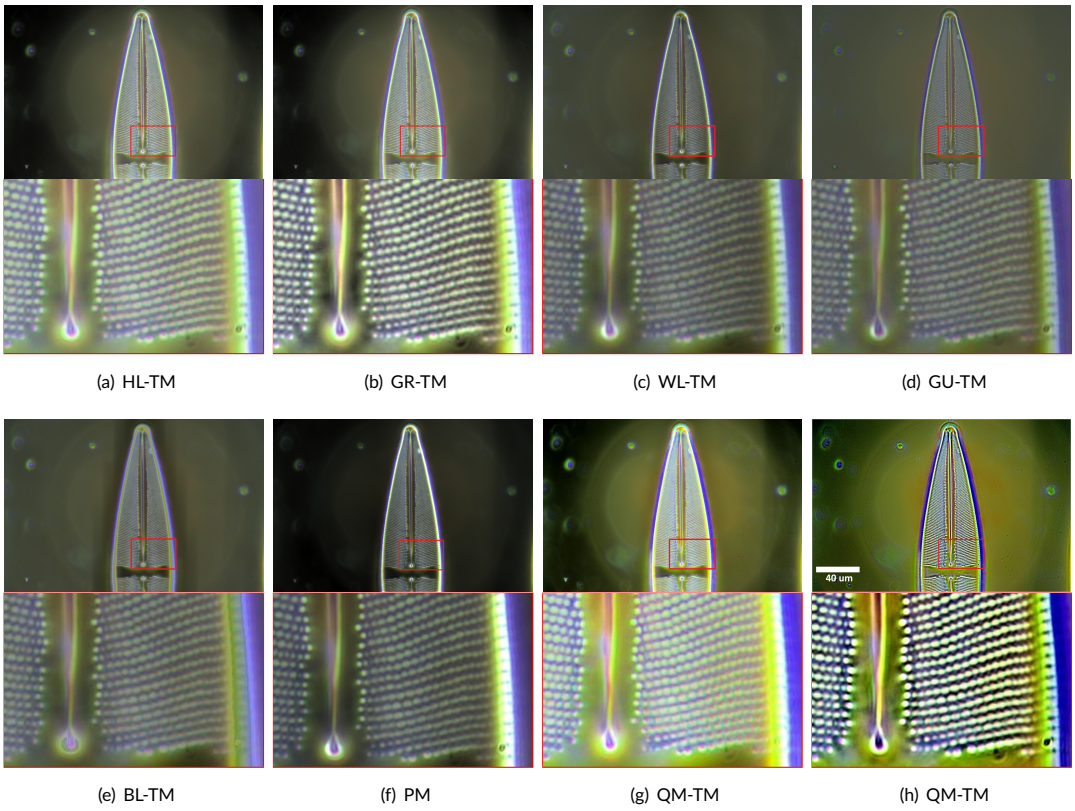

(a) HL-TM (b) GR-TM (c) WL-TM (d) GU-TM

(e) BL-TM (f) PM (g) QM-TM (h) QM-TM

FIGURE 6 Visual comparison of six state-of-the-art TMO, and one commercial HDR and tone mapping tool for "*Stauroneis gracilis*" diatom species. The closeup is placed at the bottom of different tone mapped images so that accentuation of immanent fine structures can be visualized with better clarity when the regulation of color channels is carried out separately.

where K is a normalization factor, which is given by

$$K(T) = max Pdf_N(T), Pdf_B(T) \tag{14}$$

For objective evaluation, 10 microscopy data sets are randomly selected. As shown in Table 2-4, the metric values have been generated for 8 approaches including the proposed NT-TM method. The best metric value we found are shown in bold number. As it can be observed from the Table 2 NT-TM provides the highest metric values for most of the experiments except for "*Pinnularia sp.*" and "*Frustulia saxonica*" data sets. It is observed that GR-TM has performed well in terms of TMQI for these two data sets. The metric values of SF tabulated in 3 shows that the NT-TM has obtained best score in terms of SF for 7 data sets. In terms of SF, QM-TM has shown some performance for "*Pleurosira sp.*" and "*Gyrosigma cf. balticum*", and GR-TM is giving best metric value for "*Frustulia saxonica*". Furthermore, it can be observed from Table 4 that NT-TM is giving best score values in terms of SN for 8 data sets. For other two data sets (i.e. "*Triceratium favus*" and "*Frustulia saxonica*"), WL-TM and GR-TM are giving the best score in terms of SN. From

TABLE 2 Comprehensive quantitative analysis of weighted least squares based TMO (WL-TM), gradient domain TMO (GR-TM), guided filter based TMO (GU-TM), quadrature mirror filters based TMO (QM-TM), bilateral filter based TMO (BL-TM), Hybrid L1-L0 based TMO (HL-TM), Photomatix Essentials (PM) and proposed NSCT based TMO (NT-TM) using tone-mapped image quality index (TMQI) for 10 microscopy HDR image data sets.

Image	QM-TM	HL-TM	GR-TM	WL-TM	GU-TM	BL-TM	PM	NT-TM
Lyrella sp.	0.825	0.805	0.846	0.668	0.660	0.645	0.601	**0.874**
Stauroneis gracilis	0.735	0.668	0.714	0.546	0.514	0.524	0.505	**0.756**
Triceratium favus	0.758	0.828	0.792	0.870	0.831	0.792	0.853	**0.798**
Pinnularia sp.	0.775	0.808	**0.825**	0.713	0.66	0.688	0.643	0.811
Stauroneis gracilis and Lyrella sp.	0.749	0.773	0.735	0.648	0.630	0.626	0.656	**0.806**
Pleurosira sp.	0.779	0.801	0.810	0.737	0.702	0.705	0.743	**0.827**
Frustulia saxonica	0.824	0.818	**0.945**	0.824	0.796	0.803	0.733	0.850
Lyrella sp. in-focus	0.762	0.732	0.757	0.718	0.696	0.684	0.853	**0.777**
Gyrosigma cf. balticum	0.789	0.771	0.746	0.655	0.607	0.633	0.822	**0.824**
Surirella gemma	0.774	0.755	0.741	0.641	0.604	0.624	0.772	**0.796**
Average Score	0.777	0.776	0.791	0.702	0.67	0.672	0.718	**0.812**

Table 2, Table 3 and Table 4, we can observe that the average scores for all 10 data sets, NT-TM has best values in terms of TMQI, SF and SN, respectively. This proves that, relative to the other seven tone mapping methods, the proposed NT-TM method has outperformed in terms of Structural Fidelity and Statistical Naturalness.

4 | DISCUSSION AND CONCLUSION

We propose a novel method to compress the dynamic range of microscopic HDR images of diatom species. The method is based on NSCT decomposition that improve the structural fidelity and overall quality in the tone mapped images. The multi-scale decomposition capability of NSCT not only preserve details in intricate silica-based cell walls, but also creates gain map function that helps to manipulate tonal range at multiple scales. The experimental results are compared with six state-of-the-art leading methods and one commercial tone mapping tool. The qualitative and quantitative analysis show that the proposed approach can produce superior quality LDR image (i.e. 8-bit image) than other tone mapping methods. To have a close look at the tone mapping results, we can observe that the details in ultrahigh contrast regions and low contrast regions are accurately reproduced with much higher clarity.

The proposed method opens the door to enhance color and fine details when the specimens with transparent or semitransparent nature are examined using microscopy techniques. The proposed tone-mapping procedure is carried out when the HDR image is constructed from a specimen photographed using multi-exposure imaging technique. In the resultant tone mapped image, more details are recognizable than the single optimally exposed image. These promising findings demonstrate the potential of the proposed method as one of the initial attempts at the identification and classification of different species. Future study includes hardware utilization for range compression based on multi-scale decomposition. Incorporating more efficient multi-scale decomposition implementation into the proposed

TABLE 3 Comprehensive quantitative analysis of weighted least squares based TMO (WL-TM), gradient domain TMO (GR-TM), guided filter based TMO (GU-TM), quadrature mirror filters based TMO (QM-TM), bilateral filter based TMO (BL-TM), Hybrid L1-L0 based TMO (HL-TM), Photomatix Essentials (PM) and proposed NSCT based TMO (NT-TM) using Structural Fidelity (SF) for 10 microscopy HDR image data sets.

Image	QM-TM	HL-TM	GR-TM	WL-TM	GU-TM	BL-TM	PM	NT-TM
Lyrella sp.	0.746	0.736	0.787	0.478	0.457	0.435	0.394	**0.819**
Stauroneis gracilis	0.653	0.524	0.641	0.273	0.224	0.239	0.212	**0.703**
Triceratium favus	0.775	0.749	0.854	0.774	0.685	0.708	0.878	**0.889**
Pinnularia	0.855	0.842	0.884	0.617	0.485	0.658	0.323	**0.859**
Stauroneis gracilis and Lyrella sp.	0.759	0.759	0.794	0.456	0.420	0.430	0.395	**0.799**
Pleurosira sp.	**0.818**	0.739	0.786	0.669	0.582	0.621	0.740	0.797
Frustulia saxonica	0.848	0.882	**0.889**	0.771	0.676	0.759	0.577	0.752
Lyrella sp. in-focus	0.829	0.722	0.809	0.597	0.540	0.550	**0.878**	0.799
Gyrosigma cf. balticum	**0.865**	0.719	0.659	0.482	0.379	0.445	0.810	0.818
Surirella gemma	0.868	0.783	0.709	0.448	0.371	0.419	0.806	**0.870**
Average Score	0.801	0.746	0.781	0.557	0.482	0.526	0.601	**0.812**

TABLE 4 Comprehensive quantitative analysis of weighted least squares based TMO (WL-TM), gradient domain TMO (GR-TM), guided filter based TMO (GU-TM), quadrature mirror filters based TMO (QM-TM), bilateral filter based TMO (BL-TM), Hybrid L1-L0 based TMO (HL-TM), Photomatix Essentials (PM) and proposed NSCT based TMO (NT-TM) using Statistical Naturalness (SN) for 10 microscopy HDR image data sets.

Image	QM-TM	HL-TM	GR-TM	WL-TM	GU-TM	BL-TM	PM	NT-TM
Lyrella sp.	0.340	0.257	0.156	0.063	0.066	0.048	0.019	**0.671**
Stauroneis gracilis	0.073	0.017	0.024	0.008	0.007	0.007	0.006	**0.101**
Triceratium favus	0.030	0.348	0.064	**0.547**	0.473	0.016	0.290	0.200
Pinnularia sp.	0.018	0.131	0.156	0.045	0.031	0.016	0.257	**0.288**
Stauroneis gracilis and Lyrella sp.	0.019	0.092	0.023	0.034	0.026	0.007	0.150	**0.174**
Pleurosira sp.	0.056	0.224	0.210	0.064	0.045	0.018	0.020	**0.315**
Frustulia saxonica	0.090	0.133	**0.815**	0.296	0.300	0.215	0.162	0.466
Lyrella sp. in-focus	0.006	0.008	0.007	0.082	0.076	0.028	0.29	**0.085**
Gyrosigma cf. balticum	0.045	0.128	0.107	0.027	0.017	0.010	0.217	**0.298**
Surirella gemma	0.008	0.018	0.037	0.023	0.018	0.014	0.046	**0.121**
Average Score	0.069	0.136	0.160	0.119	0.106	0.038	0.146	**0.271**

workflow has great potential in developing real time systems for detail enhancement of low-contrast nano- and micro-structures, which is specially suitable for visualizing transparent specimens such as diatoms.

Acknowledgments

This work was supported in part by the Spanish Government under the Aqualitas-retos project (Ref.CTM2014-51907-C2-2- R-MINECO).

Conflict of Interest

The authors declare no conflict of interest.

references

[1] Durand F, Dorsey J. Fast Bilateral Filtering for the Display of High-Dynamic-Range Images. ACM Trans Graph 2002 Jul;21(3):257–266.

[2] El Mezeni DM, Saranovac LV. Enhanced local tone mapping for detail preserving reproduction of high dynamic range images. Journal of Visual Communication and Image Representation 2018;53:122 – 133.

[3] Debevec PE, Malik J. Recovering High Dynamic Range Radiance Maps from Photographs. In: Proceedings of the 24th Annual Conference on Computer Graphics and Interactive Techniques SIGGRAPH '97, USA: ACM Press/Addison-Wesley Publishing Co.; 1997. p. 369–378.

[4] Larson GW, Rushmeier H, Piatko C. A visibility matching tone reproduction operator for high dynamic range scenes. IEEE Transactions on Visualization and Computer Graphics 1997;3(4):291–306.

[5] Yang DXD, El Gamal A, Fowler B, Hui Tian. A 640/spl times/512 CMOS image sensor with ultra wide dynamic range floating-point pixel-level ADC. In: 1999 IEEE International Solid-State Circuits Conference. Digest of Technical Papers. ISSCC. First Edition (Cat. No.99CH36278); 1999. p. 308–309.

[6] HDRSoft:Photomatix; 2008. http://www.hdrsoft.com.

[7] Okonek B: Easy HDR, always properly exposed images by exposure blending and tone mapping; 2006. http://www.easyhdr.com/index.php.

[8] SchomannA: FDRTools; 2012. http://www.fdrtools.com.

[9] Mehl M: Picturenaut, HDRI-generator, tone mapping; 2008. http://www.hdrlabs.com/picturenaut/index.html.

[10] Kinoshita Y, Kiya H. iTM-Net: Deep Inverse Tone Mapping Using Novel Loss Function Considering Tone Mapping Operator. IEEE Access 2019;7:73555–73563.

[11] Piper J. Image processing for the optimization of dynamic range and ultra-high contrast amplification in photomicrography. Modern Research and Educational Topics in Microscopy, Formatex Research Center, Badajoz, Spain 2010;p. 1436–1444.

[12] Gröger P, Poulsen N, Klemm J, Kröger N, Schlierf M. Establishing super-resolution imaging for proteins in diatom biosilica. Scientific Reports 2016;6(1):36824.

[13] Sánchez C, Cristóbal G, Bueno G. Diatom identification including life cycle stages through morphological and texture descriptors. PeerJ 2019;7:e6770.

[14] Singh H, Cristóbal G, Kumar V. In: Cristóbal G, Blanco S, Bueno G, editors. Multifocus and Multiexposure Techniques Cham: Modern Trends in Diatom Identification: Fundamentals and Applications, Springer International Publishing; 2020. p. 165–181.

[15] Miao D, Zhu Z, Bai Y, Jiang G, Duan Z. Novel Tone Mapping Method via Macro-Micro Modeling of Human Visual System. IEEE Access 2019;7:118359–118369.

[16] Chiu K, Herf M, Shirley P, Swamy S, Wang C, Zimmerman K. Spatially Nonuniform Scaling Functions for High Contrast Images. In: In Proceedings of Graphics Interface '93; 1993. p. 245–253.

[17] Reinhard E, Stark M, Shirley P, Ferwerda J. Photographic Tone Reproduction for Digital Images. ACM Trans Graph 2002 Jul;21(3):267–276. https://doi.org/10.1145/566654.566575.

[18] Choudhury P, Tumblin J. The Trilateral Filter for High Contrast Images and Meshes. In: ACM SIGGRAPH 2005 Courses SIGGRAPH '05, New York, NY, USA: Association for Computing Machinery; 2005. p. 5–es.

[19] Farbman Z, Fattal R, Lischinski D, Szeliski R. Edge-Preserving Decompositions for Multi-Scale Tone and Detail Manipulation. ACM Trans Graph 2008 Aug;27(3):1–10.

[20] Bansal N, Raman S. Regularized tone mapping using edge preserving filters. In: 2015 Twenty First National Conference on Communications (NCC); 2015. p. 1–6.

[21] Fattal R, Lischinski D, Werman M. Gradient Domain High Dynamic Range Compression. ACM Trans Graph 2002 Jul;21(3):249–256.

[22] Wang T, Ke W, Zwao D, Chen F, Chiu C. Block-Based Gradient Domain High Dynamic Range Compression Design for Real-Time Applications. In: 2007 IEEE International Conference on Image Processing, vol. 3; 2007. p. III – 561–III – 564.

[23] Khan IR, Rahardja S, Khan MM, Movania MM, Abed F. A Tone-Mapping Technique Based on Histogram Using a Sensitivity Model of the Human Visual System. IEEE Transactions on Industrial Electronics 2018;65(4):3469–3479.

[24] Drago F, Myszkowski K, Annen T, Chiba N. Adaptive Logarithmic Mapping For Displaying High Contrast Scenes. Computer Graphics Forum 2003;22:419–426.

[25] Jung C, Xu K. Naturalness-preserved tone mapping in images based on perceptual quantization. In: 2017 IEEE International Conference on Image Processing (ICIP); 2017. p. 2403–2407.

[26] Lee DH, Fan M, Kim SW, Kang MC, Ko SJ. High dynamic range image tone mapping based on asymmetric model of retinal adaptation. Signal Processing: Image Communication 2018;68:120 – 128.

[27] Mantiuk R, Daly S, Kerofsky L. Display Adaptive Tone Mapping. ACM Trans Graph 2008 Aug;27(3):1–10.

[28] Da Cunha AL, Zhou J, Do MN. The Nonsubsampled Contourlet Transform: Theory, Design, and Applications. IEEE Transactions on Image Processing 2006;15(10):3089–3101.

[29] Piper J. In: Cristóbal G, Blanco S, Bueno G, editors. Light Filtering in Microscopy Cham: Modern Trends in Diatom Identification: Fundamentals and Applications, Springer International Publishing; 2020. p. 95–111.

[30] Heeger DJ. Half-squaring in responses of cat striate cells. Visual Neuroscience 1992;9(5):427–443.

[31] Lee HC. Automatic tone adjustment by contrast gain-control on edges. United States Patent 2001;6285798.

[32] Li Y, Sharan L, Adelson EH. Compressing and Companding High Dynamic Range Images with Subband Architectures. In: ACM SIGGRAPH 2005 Papers SIGGRAPH '05, New York, NY, USA: Association for Computing Machinery; 2005. p. 836–844.

[33] Hildebrand M, Lerch SJL, Shrestha RP. Understanding Diatom Cell Wall Silicification—Moving Forward. Frontiers in Marine Science 2018;5:125.

[34] He K, Sun J, Tang X. Guided Image Filtering. IEEE Transactions on Pattern Analysis and Machine Intelligence 2013;35(6):1397–1409.

[35] Liang Z, Xu J, Zhang D, Cao Z, Zhang L. A Hybrid l1-l0 Layer Decomposition Model for Tone Mapping. In: 2018 IEEE/CVF Conference on Computer Vision and Pattern Recognition; 2018. p. 4758–4766.

[36] Yeganeh H, Wang Z. Objective Quality Assessment of Tone-Mapped Images. IEEE Transactions on Image Processing 2013;22(2):657–667.